J|A|C|S
ARTICLES
Published on Web 09/09/2004

Unusual Ar−H/Rh−H J_{HH} NMR Coupling in Complexes of Rhodium(III): Experimental Evidence and Theoretical Support for an η^1−Arene Structure

Jennifer R. Krumper,[†] Michael Gerisch,[†] Alessandra Magistrato,[‡] Ursula Rothlisberger,*[,§] Robert G. Bergman,*[,†] and T. Don Tilley*[,†]

Contribution from the Department of Chemistry, University of California and Division of Chemical Sciences, Lawrence Berkeley National Laboratory, Berkeley, California 94702, International School for Advanced Studies (ISAS/SISSA) and INFM-Democritos Center, Trieste 34140, Italy, and Laboratory of Computational Chemistry & Biochemistry, BCH 4109 EPFL, Lausanne CH-1015 Switzerland

Received April 22, 2004; Revised Manuscript Received July 2, 2004; E-mail: ursula.roethlisberger@epfl.ch; bergman@cchem.berkeley.edu; tdtilley@socrates.berkeley.edu

Abstract: The synthesis and structural properties of three new hydridorhodium(III) complexes are reported. Hydrogenolysis of the cyclometalated rhodium dichloride complexes [$RhCl_2${(*S*,*S*)-benbox(Me_2)}] (**2a**−**c**) leads to formation of the new complexes [$RhCl_2$(H){(*S*,*S*)-ip-benbox(Me_2)H}] (**3a**−**c**) in 45% to 85% yield. Compounds **3a**−**c** were found to have unusual features by NMR spectroscopy: in particular, downfield shifted aryl proton resonances (8.88−9.03 ppm) that were coupled to the rhodium hydride resonances. Using X-ray crystallographic studies, a variety of solid- and solution-state characterization techniques, and DFT calculations, these features were attributed to the presence of weak π-type η^1-arene interactions in **3a**−**c**.

Introduction

The formation of dative bonds between hydrocarbons and metals is a critical step in many metal-catalyzed organic reactions and is a subject of fundamental importance.[1−9] Of the many hydrocarbons that bind to metals, arenes offer the most diverse modes of interaction and some of the most important applications. Metal−arene binding has been shown to be a critical component of many important reactions, including dearomatization and aromatic substitution.[10−15] As arenes can provide up to 6 π electrons for bonding, metal−arene complexes of all possible hapticities are known (η^1−η^6).[16] Additionally, arenes can interact via their σ-bonding framework to form η^2−C−H agostic complexes.[17−23]

One of the least common forms of metal−arene interaction is η^1−arene coordination.[16] Due to the relative ease of formation of η^2−arene complexes, most metals that bind arenes do so with higher hapticity. As such, η^1−arene coordination has been reported for a limited number of transition metals.[24−29] These transition metal-based complexes are related to the Wheland intermediates formed during electrophilic aromatic substitution reactions.[30]

[†] University of California.
[‡] Present address: International School for Advanced Studies.
[§] Laboratory of Computational Chemistry and Biochemistry.

(1) Hall, C.; Perutz, R. N. *Chem. Rev.* **1996**, *96*, 3125−3146.
(2) Brookhart, M.; Green, M. L. H. *J. Organomet. Chem.* **1980**, *250*, 395−408.
(3) Brookhart, M.; Green, M. L. H.; Wong, L. L. *Prog. Inorg. Chem.* **1988**, *36*, 1−124.
(4) Jordan, R. F. *Adv. Organomet. Chem.* **1991**, *32*, 325−387.
(5) Cossee, P. *J. Catal.* **1964**, *3*, 80−88.
(6) Arlman, E. J.; Cossee, P. *J. Catal.* **1964**, *3*, 99−104.
(7) Leclerc, M. K.; Brintzinger, H. H. *J. Am. Chem. Soc.* **1995**, *117*, 1651−1652.
(8) Periana, R. A.; Bergman, R. G. *J. Am. Chem. Soc.* **1986**, *108*, 7332−7346.
(9) Northcutt, T. O.; Wick, D. D.; Vetter, A. J.; Jones, W. D. *J. Am. Chem. Soc.* **2001**, *123*, 7257−7270.
(10) Jones, W. D.; Feher, F. J. *J. Am. Chem. Soc.* **1984**, *106*, 1650−1663.
(11) Johansson, L.; Tilset, M.; Labinger, J. A.; Bercaw, J. E. *J. Am. Chem. Soc.* **2000**, *122*, 10846−10855.
(12) Reinartz, S.; White, P. S.; Brookhart, M.; Templeton, J. L. *J. Am. Chem. Soc.* **2001**, *123*, 12724−12725.
(13) Norris, C. M.; Reinartz, S.; White, P. S.; Templeton, J. L. *Organometallics* **2002**, *21*, 5649−5656.
(14) Brooks, B. C.; Gunnoe, T. B.; Harman, W. D. *Coord. Chem. Rev.* **2000**, *206*, 3−61.
(15) Harman, W. D. *Chem. Rev.* **1997**, *97*, 1953−1978.
(16) Hubig, S. M.; Lindeman, S. V.; Kochi, J. K. *Coord. Chem. Rev.* **2000**, *200*, 831−873.
(17) Vigalok, A.; Uzan, O.; Shimon, L. J. W.; Ben-David, Y.; Martin, J. M. L.; Milstein, D. *J. Am. Chem. Soc.* **1998**, *120*, 12539−12544.
(18) Aryl C−H agostic interactions with a nonpincer ligand: Rybtchinski, B.; Cohen, R.; Ben-David, Y.; Martin, J. M. L.; Milstein, D. *J. Am. Chem. Soc.* **2003**, *125*, 11041−11050.
(19) Gusev, D. G.; Madott, M.; Dolgushin, F. M.; Lyssenko, K. A.; Antipin, M. Y. *Organometallics* **2000**, *19*, 1734−1739.
(20) Dani, P.; Toorneman, M. A. M.; van Klink, G. P. M.; van Koten, G. *Organometallics* **2000**, *19*, 5287−5296.
(21) Steenwinkel, P.; Kolmschot, S.; Gossage, R. A.; Dani, P.; Veldman, N.; Spek, A. L.; van Koten, G. *Eur. J. Inorg. Chem.* **1998**, 477−483.
(22) Dani, P.; Karlen, T.; Gossage, R. A.; Smeets, W. J. J.; Spek, A. L.; van Koten, G. *J. Am. Chem. Soc.* **1997**, *119*, 11317−11318.
(23) van der Boom, M. E.; Iron, M. A.; Atasoylu, O.; Shimon, L. J. W.; Rozenberg, H.; Ben-David, Y.; Milstein, D. *Inorg. Chim. Acta* **2004**, *357*, 1854−1864.
(24) Reid, S. M.; Boyle, R. C.; Mague, J. T.; Fink, M. J. *J. Am. Chem. Soc.* **2003**, *125*, 7816−7817.
(25) Geldbach, T. J.; Drago, D.; Pregosin, P. S. *J. Organomet. Chem.* **2002**, *643*, 214−222.
(26) Chen, H.; Bartlett, R. A.; Olmstead, M. M.; Power, P. P.; Shoner, S. C. *J. Am. Chem. Soc.* **1990**, *112*, 1048−1055.
(27) Albrecht, M.; Spek, A. L.; van Koten, G. *J. Am. Chem. Soc.* **2001**, *123*, 7233−7246.
(28) Lau, W.; Huffman, J. C.; Kochi, J. K. *J. Am. Chem. Soc.* **1982**, *104*, 5515−5517.

10.1021/ja047665b CCC: $27.50

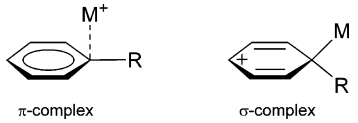

Figure 1. Cationic σ- and π-type η^1−arene complexes. Figure adapted from Hubig, S. M.; Lindeman, S. V.; Kochi, J. K. *Coord. Chem. Rev.* **2000**, *200*, 831.

For both metallic and nonmetallic electron acceptors, η^1−arene complexes are grouped into two general classes: σ-type complexes and π-type complexes (Figure 1).[31] In σ-complexes, a high degree of charge transfer from the arene to the coordinated electron-acceptor occurs, involving significant rehybridization of the *ipso* carbon from sp^2 to sp^3 and concomitant geometric distortion of the arene ring. Wheland complexes, involving hard cations (e.g., Cl^+,[32] H^+,[30] and CH_3^+ [33]) are of this class. In contrast, softer electron-acceptors (e.g., Ag^+,[34] Si^+,[35] Ru(II),[25] and Pd(0)[24]) can form π-type complexes with arenes. The geometries of these complexes involve largely unperturbed arene rings, and such complexes are quite rare.

This paper describes a series of new rhodium(III) pincer ligand complexes that display unusual intramolecular π-type η^1−arene interactions between the metal center and the arene ring of an NCN pincer ligand and an otherwise coordinatively unsaturated metal center. Experimental and theoretical probes were used to explore the nature of these interactions in both the solid and solution states. To our knowledge, these complexes represent the first examples of η^1−arene coordination to rhodium centers.

Results

Synthesis and Spectroscopic Characterization of 3a−c. We have recently reported the synthesis and reaction chemistry of a family of rhodium(II) (**1**) and rhodium(III) (**2**) complexes of C_2-symmetric bis(oxazoline) ligands.[36,37] In the context of these studies, we observed that the rhodium(II) complex bearing four methyl groups on its bis(oxazoline) ligand (**1c**) underwent disproportionation to form two rhodium(III) complexes: **2c** and a new rhodium(III) hydride complex (**3c**) (eq 1).

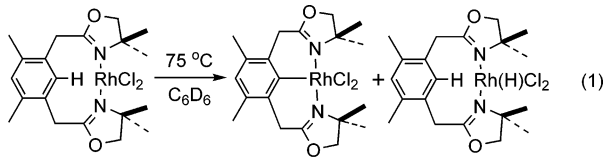

(1)

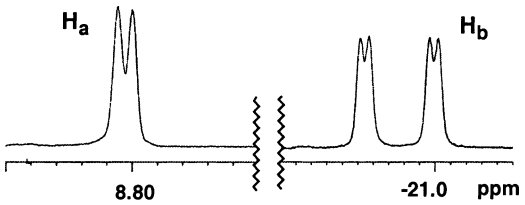

Figure 2. ^{1}H NMR data for **3a**.

The initially observed hydride complex **3c** was synthesized independently by hydrogenolysis, in a manner analogous to that reported by Milstein and Fryzuk.[38−41] This methodology proved quite general, and treatment of benzene solutions of **2a**−**c** with H_2 resulted in overall addition of H_2 across the Rh−C_{aryl} bonds to form the hydride complexes **3a** (85%), **3b** (45%), and **3c** (75%) (eq 2).

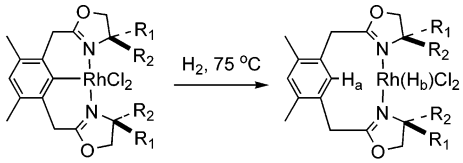

(2)

The ^{1}H NMR spectra of complexes **3a**−**c** show several surprising features associated with the (formerly) *ipso*-aryl (H_a) and rhodium-hydride (H_b) resonances. The rhodium-hydride resonances (H_b) in **3a**−**c** appear at −20.76 (**3a**, dd, J_{H-H} = 2.5 Hz, $^1J_{Rh-H}$ = 22.1 Hz), −20.81 (**3b**, dd, J_{H-H} = 3.1 Hz, $^1J_{Rh-H}$ = 22.1 Hz), and −19.70 (**3c**, dd, J_{H-H} = 3.3 Hz, $^1J_{Rh-H}$ = 18.8 Hz) ppm. The resonances for H_b exhibit coupling to the rhodium nucleus and unexpected coupling to H_a (Figure 2). The surprising H_a−H_b coupling was confirmed by homonuclear decoupling and ^{1}H−^{1}H TOCSY experiments performed on **3b**. Interestingly, the H_a resonances appear quite far downfield, giving rise to doublet peaks at 8.88 (**3a**, J_{H-H} = 2.5 Hz), 8.90 (**3b**, J_{H-H} = 3.1 Hz), and 9.03 (**3c**, J_{H-H} = 3.3 Hz) ppm. These peaks represent an average shift of $\Delta\delta$ = 1.75 ppm downfield from the *para* protons on the aromatic rings, and an average shift of $\Delta\delta$ = 1.78 ppm downfield from the H_a protons in the free ligands.

The coupling of the proximal aryl protons (H_a) to the rhodium hydride resonances (H_b) initially suggested the presence of agostic interactions between the aryl C_a−H_a bonds and the rhodium centers in these complexes. Several pieces of data were found to be inconsistent with this hypothesis, however. First, in complexes **3a**−**c** the H_a resonances are shifted significantly *downfield* relative to the corresponding signals of the free ligands; typically agostic coordination of a C−H bond results in an *upfield* shift of the relevant proton.[2] *Second, no Rh−H_a coupling was observed in the ^{1}H NMR spectra of these complexes.* To address whether the absence of rhodium coupling was due to relaxation of the rhodium nucleus at high field strength, a ^{1}H NMR spectrum of **3b** was acquired on a 90 MHz

(29) Batsanov, A. S.; Crabtree, S. P.; Howard, J. A. K.; Lehmann, C. W.; Kilner, M. *J. Organomet. Chem.* **1998**, *550*, 59−61.
(30) Reed, C. A.; Kim, K. C.; Stoyanov, E. S.; Stasko, D.; Tham, F. S.; Mueller, L. J.; Boyd, P. D. W. *J. Am. Chem. Soc.* **2003**, *125*, 1796−1804.
(31) Many complexes are believed to lie in a continuum between these two cannonical extremes. For discussions of this subject, see Hubig et al.[16] and Reed et al.[30]
(32) Rathore, R.; Hecht, J.; Kochi, J. K. *J. Am. Chem. Soc.* **1998**, *120*, 13278−13279.
(33) Allen, F. H.; Kennard, O.; Watson, D. G.; Brammer, L.; Orpen, A. G.; Taylor, R. *J. Chem. Soc., Perkin Trans. 2* **1987**, S1−S19.
(34) Mascal, M.; Hansen, J.; Blake, A. J.; Li, W. S. *Chem. Commun.* **1998**, 355−356.
(35) Although silicenium ion is not strictly "soft", a π-type complex is formed: Lambert, J. B.; Zhang, S. Z.; Ciro, S. M. *Organometallics* **1994**, *13*, 2430−2443.
(36) Gerisch, M.; Krumper, J. R.; Bergman, R. G.; Tilley, T. D. *J. Am. Chem. Soc.* **2001**, *123*, 5818−5819.
(37) Gerisch, M.; Krumper, J. R.; Bergman, R. G.; Tilley, T. D. *Organometallics* **2003**, *22*, 47−58.
(38) Liou, S. Y.; Gozin, M.; Milstein, D. *Chem. Commun.* **1995**, 1965−1966.
(39) Liou, S. Y.; van der Boom, M. E.; Milstein, D. *Chem. Commun.* **1998**, 687−688.
(40) Fryzuk, M. D.; MacNeil, P. A.; Rettig, S. J. *J. Am. Chem. Soc.* **1987**, *109*, 2803−2812.
(41) Fryzuk, M. D.; Montgomery, C. D.; Rettig, S. J. *Organometallics* **1991**, *10*, 467−473.

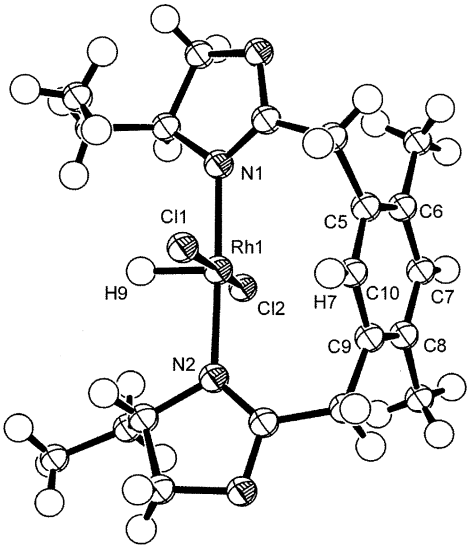

Figure 3. ORTEP drawing of the molecular structure of **3a**. Thermal ellipsoids are shown at the 50% probability level.

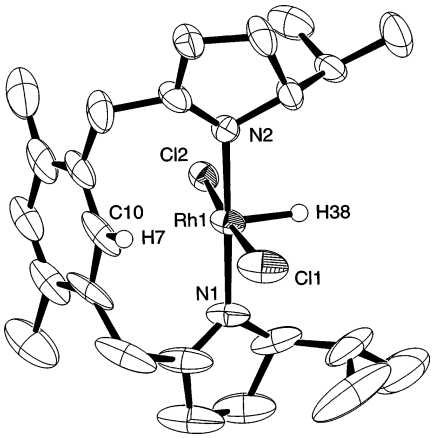

Figure 4. ORTEP drawing of the molecular structure of **3b**. Hydrogen atoms (except for H7 and H38) are omitted for clarity. Thermal ellipsoids are shown at the 50% probability level.

NMR instrument. As with the spectra acquired at 300−500 MHz, this spectrum showed no Rh−H_a coupling. Third, no Rh−C_a coupling was observed in the $^{13}C\{^1H\}$ spectra of **3a**−**c** or in the 2D $^1H-^{13}C$ HMQC spectrum of **3b**. Both Rh−H_a and Rh−C_a coupling would be expected for agostic interactions between the aryl C_a-H_a bond and the rhodium centers in **3a**−**c**.[42,43] Interestingly, the $^{13}C\{^1H\}$ NMR chemical shifts of the C_a carbons in **3a**−**c** were found to be shifted slightly upfield (**3a**, 118.5; **3b**, 121.5; **3c**, 121.6) relative to the other aryl carbons in these complexes ($\delta = 128-140$ ppm). Finally, no IR stretches consistent with an agostic C−H bond ($\upsilon_{CH} = 2700-2850$ cm^{-1}) were observed for complexes **3a**−**c**.[2,3]

One reliable indication of the presence of an agostic interaction is a reduction in the coupling constant of the C−H bond involved.[2,3] The aryl C_a-H_a coupling constant for **3b**, measured in the ^{13}C NMR spectrum, is 158 Hz. This value is indicative of an unperturbed sp^2 hybridized aryl C−H bond (for C_6H_6, $^1J_{C-H} = 159$ Hz), and is atypical for an agostic C−H bond.[44] For comparison, in two closely related PCP pincer ruthenium hydride complexes described by Gusev et al.,[19] the C−H coupling constants were estimated to be very low: 52 and 58 Hz. Milstein et al.[17] have described an aryl-agostic rhodium PCP pincer complex that features a C−H coupling constant of 123 Hz for the agostic C−H bond. Interestingly, although Rh−H coupling was observed in the agostic aryl proton analogous to H_a ($J_{Rh-H} = 18.1$ Hz) in Milstein's complex, no Rh−C coupling was observed for the agostic carbon in the ^{13}C NMR spectrum.

X-ray Crystal Structures. The NMR data obtained for complexes **3a**−**c** indicate that despite the existence of H_a-H_b coupling, traditional agostic interactions are not present in these complexes. Further support for this conclusion was drawn from

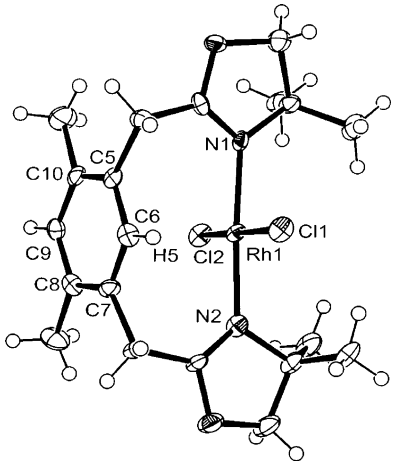

Figure 5. ORTEP drawing of the molecular structure of **3c**. Thermal ellipsoids are shown at the 50% probability level.

Table 1. Selected Interatomic Distances (Å) and Bond Angles (degrees) for [$RhHCl_2$\{et-benbox(Me_2)\}] (**3a**)

Rh(1)−H(9)	**1.43(3)**	Cl(1)−Rh(1)−Cl(2)	**176.68(3)**
C(9)−C(10)	**1.397(5)**	N(1)−Rh(1)−N(2)	**177.8(1)**
C(10)−C(5)	**1.391(4)**	C(5)−C(10)−C(9)	**121.6(3)**
C(5)−C(6)	**1.388(5)**	C(6)−C(5)−C(10)	**119.4(3)**
C(6)−C(7)	**1.392(5)**	C(5)−C(6)−C(7)	**118.0(3)**
C(7)−C(8)	**1.393(5)**	C(6)−C(7)−C(8)	**123.6(3)**
C(8)−C(9)	**1.396(4)**	C(7)−C(8)−C(9)	**117.4(3)**
Rh(1)···C(10)	**2.622(3)**	C(8)−C(9)−C(10)	**119.6(3)**

Table 2. Selected Interatomic Distances (Å) and Bond Angles (deg) for [$RhHCl_2$\{ip-benbox(Me_2)\}] (**3b**)

Rh(1)−H(38)	**1.47(5)**	Cl(1)−Rh(1)−Cl(2)	**174.93(7)**
C(9)−C(10)	**1.39(1)**	N(1)−Rh(1)−N(2)	**178.2(2)**
C(10)−C(5)	**1.42(1)**	C(5)−C(10)−C(9)	**122.4(8)**
C(5)−C(6)	**1.39(1)**	C(6)−C(5)−C(10)	**116.6(9)**
C(6)−C(7)	**1.38(1)**	C(5)−C(6)−C(7)	**120.0(8)**
C(7)−C(8)	**1.39(1)**	C(6)−C(7)−C(8)	**123.9(8)**
C(8)−C(9)	**1.40(1)**	C(7)−C(8)−C(9)	**116.5(9)**
Rh(1)···C(10)	**2.632(6)**	C(8)−C(9)−C(10)	**120.1(8)**

Table 3. Selected Interatomic Distances (Å) and Bond Angles (deg) for [$RhHCl_2$\{dm-benbox(Me_2)\}] (**3c**)

C(9)−C(10)	**1.398(9)**	N(1)−Rh(1)−N(2)	**176.1(2)**
C(10)−C(5)	**1.385(9)**	C(5)−C(10)−C(9)	**118.0(6)**
C(5)−C(6)	**1.39(1)**	C(6)−C(5)−C(10)	**119.5(6)**
C(6)−C(7)	**1.380(9)**	C(5)−C(6)−C(7)	**121.5(6)**
C(7)−C(8)	**1.39(1)**	C(6)−C(7)−C(8)	**119.8(6)**
C(8)−C(9)	**1.382(9)**	C(7)−C(8)−C(9)	**118.0(6)**
Rh(1)···C(6)	**2.608(7)**	C(8)−C(9)−C(10)	**123.0(6)**

(42) Vigalok, A.; Ben-David, Y.; Milstein, D. *Organometallics* **1996**, *15*, 1839−1844.
(43) Rybtchinski, B.; Vigalok, A.; Ben-David, Y.; Milstein, D. *J. Am. Chem. Soc.* **1996**, *118*, 12406−12415.
(44) Green, R. D. *Hydrogen Bonding by C−H Groups*; Macmillan: London, 1974.

Table 4. Crystal Data and Structure Refinement for **3a**, **3b**, and **3c**

	3a	3b	3c
empirical formula	$C_{20}H_{29}Cl_2N_2O_2Rh$	$C_{22}H_{33}Cl_2N_2O_2Rh{\cdot}C_7H_8$	$C_{20}H_{29}Cl_2N_2O_2Rh$
formula weight	503.27	623.47	503.27
crystal color, habit	orange, tablet	orange, fragment	yellow, blade
crystal dimensions (mm)	0.20 0.12 0.12	0.19 0.12 0.09	0.20 0.17 0.06
crystal system	orthorhombic	monoclinic	monoclinic
lattice type	primitive	C-centered	primitive
lattice parameters (Å unless otherwise noted)	$a = 12.0307(7)$, $b = 12.9556(7)$ $c = 13.9502(8)$	$a = 20.690(3)$, $b = 8.419(1)$ $c = 16.060(2)$, $\beta = 106.887(2)°$	$a = 9.0724(7)$, $b = 12.273(1)$, $c = 9.8953(8)$, $\beta = 95.350(1)°$
V [Å^3]	2174.3(2)	2676.8(6)	1097.0(2)
space group	$P2_12_12_1$ (#19)	$C2$ (#5)	$P2_1$ (#4)
Z value	4	4	2
D_{calc}	1.537 g/cm^3	1.547 g/cm^3	1.524 g/cm^3
F_{000}	1032.00	1296.00	516.00
μ (Mo Kα)	10.46 cm^{-1}	8.66 cm^{-1}	10.37 cm^{-1}
temperature	-117 ± 1 °C	-127 ± 1 °C	-142 ± 1 °C
2θ range	3.50°−45.00°	3.50°−45.00°	5.32°−49.32°
$2\theta_{max}$	49.4°	49.4°	49.4°
no. of reflections measured	total: 9760 unique: 3601 ($R_{int} = 0.034$)	total: 5954 unique: 4060 ($R_{int} = 0.037$)	total: 4905 unique: 2105 ($R_{int} = 0.042$)
p-factor	0.0300	0.0300	0.0300
no. observations ($I > 3.00\sigma(I)$)	2923	2624	2949
no. variables	247	277	243
reflection/parameter ratio	11.83	9.47	12.14
residuals:[a] R, R_w, R_{all}	0.020, 0.022, 0.030	0.032, 0.030, 0.064	0.038, 0.044, 0.044
goodness of fit indicator	0.80	0.89	1.30

[a] $R = \Sigma\ ||F_o| - |F_c||/\Sigma\ |F_o|$, $R_w = [\Sigma w(|F_o| - |F_c|)^2/\Sigma w\ F_o^2]^{1/2}$, where $w = 1/\sigma^2(F_o)$

Table 5. Summary of Crystal Data Relevant to Interactions in **3a**−**c**

	3a	3b	3c
Rh−H_b	1.45(3)	1.47(5)	not found
Rh···H_a	2.71[a]	2.66[a]	2.69[a]
Rh···C_a	2.622(3)	2.632(6)	2.608(7)
H_a···Cl(1)	2.65[a]	2.80[a]	2.64[a]
C_a−H_a−Rh	74.30[a]	77.73[a]	75.08[a]
N−Rh−N	177.8(1)	178.2(2)	176.1(2)
Cl−Rh−Cl	176.68(3)	174.93(7)	177.06(7)

[a] Bond length or angle derived from calculated location of H_a.

crystallographic characterization of the complexes. Crystals of **3a**−**c** suitable for X-ray diffraction were obtained by cooling toluene or toluene/pentane solutions of each to −30 °C. Crystal structures of **3a**−**c** were obtained (Figures 3−5, Tables 1−3), and all three complexes were found to feature square-based pyramidal geometries[45] with *trans* arrangements of the chloride ligands. For complexes **3a** and **3b**, the rhodium-bound hydride ligand (H_b) was located and refined in the difference map, although for complex **3c**, this ligand was not found. Collection parameters and crystal data are presented in Table 4 and the metrical parameters most relevant to the H_a−Rh−H_b interaction are collected in Table 5. More complete bond length and angle data for each complex are presented in Tables 1−3.

The crystal data confirm the conclusion that traditional agostic interactions are not present in complexes **3a**−**c**. First, the C_a−Rh distances are longer than would be expected for traditional agostic interactions, and range from 2.61 to 2.63 Å (Table 1). Typical agostic C−M distances range from 1.9 to 2.5 Å,[2] although weak agostic interactions in structurally related pincer complexes have been found to feature M−C distances of 2.11 to 2.69 Å.[17,19,22,42,46,47] More surprising than the Rh−C_a distances for **3a**−**c** are the Rh−H_a distances. Although the H_a atoms were not located or refined in the difference maps, their locations were calculated based on C_a−H_a distances of 0.95 Å. These approximations are reasonable given the planarity and regularity of C−C bond distances in the aryl rings of the ligands. For complexes **3a**−**c**, the H_a−Rh distances are much longer than would be expected for agostic interactions, ranging from 2.66 to 2.71 Å (Table 5). Typical agostic H−M distances range from 1.8 to 2.2 Å,[2] and the distances observed for agostic M−H interactions in structurally related pincer complexes range from 2.11 to 2.39 Å.[17,19,22,42,46,47] A few other d^6 systems have been reported to possess long H−Rh and C−Rh distances, similar to those observed in **3a**−**c**.[48−50] However, for none of these systems were NMR characteristics similar to **3a**−**c** reported, suggesting that the interactions in **3a**−**c** are unique.

Possible Explanations for H_a−H_b Coupling and the H_a Chemical Shift. The crystallographic and spectroscopic data for complexes **3a**−**c** clearly indicate that agostic interactions are not present in these complexes, leaving four alternative hypotheses for the origin of H_a−H_b coupling (Figure 6): (a) preagostic bonding (*vide infra*),[51−60] (b) a direct through-space

(45) The flat square pyramid geometries of **3a**−**c** are typical for low spin d^6 complexes, see Albright, T. A.; Burdett, J. K.; Whangbo, M.-H. *Orbital Interactions in Chemistry*; Wiley: New York, 1985.
(46) Hamilton, D. G.; Crabtree, R. H. *J. Am. Chem. Soc.* **1988**, *110*, 4126−4133.
(47) Albeniz, A. C.; Schulte, G.; Crabtree, R. H. *Organometallics* **1992**, *11*, 242−249.
(48) La Placa, S. J.; Ibers, J. A. *Inorg. Chem.* **1965**, *4*, 778−783.
(49) Fawcett, J.; Holloway, J. H.; Saunders, G. C. *Inorg. Chim. Acta* **1992**, *202*, 111−113.
(50) Cini, R.; Cavaglioni, A. *Inorg. Chem.* **1999**, *38*, 3751−3754.
(51) Albinati, A.; Anklin, C. G.; Pregosin, P. *Inorg. Chem.* **1987**, *26*, 503−508.
(52) Albinati, A.; Arz, C.; Pregosin, P. *Inorg. Chem.* **1987**, *26*, 508−513.
(53) Albinati, A.; Pregosin, P. S.; Wombacher, F. *Inorg. Chem.* **1990**, *29*, 1812−1817.
(54) Bortolin, M.; Bucher, U. E.; Ruegger, H.; Venanzi, L. M.; Albinati, A.; Lianza, F.; Trofimenko, S. *Organometallics* **1992**, *11*, 2514−2521.
(55) Neve, F.; Ghedini, M.; Crispini, A. *Organometallics* **1992**, *11*, 3324−3327.
(56) Cano, M.; Heras, J. V.; Maeso, M.; Alvaro, M.; Fernández, R.; Pinilla, E.; Campo, J. A.; Monge, A. *J. Organomet. Chem.* **1997**, *534*, 159−172.
(57) Campo, J. A.; Cano, M.; Heras, J. V.; Pinilla, E.; Ruiz-Bermejo, M.; Torres, R. *J. Organomet. Chem.* **1999**, *582*, 173−182.
(58) Brammer, L.; Charnock, J. M.; Goggin, P. L.; Goodfellow, R. J.; Orpen, A. G.; Koetzle, T. F. *J. Chem. Soc., Dalton Trans.* **1991**, 1789−1798.
(59) Brammer, L.; Zhao, D.; Ladipo, F. T.; Braddockwilking, J. *Acta Crystallogr., Sect. B.* **1995**, *51*, 632−640.

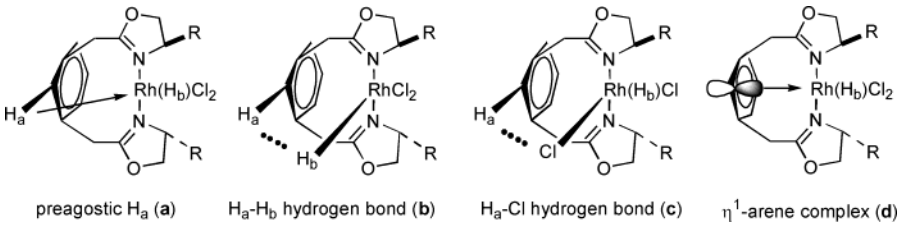

Figure 6. Possible sources of H_a-H_b coupling.

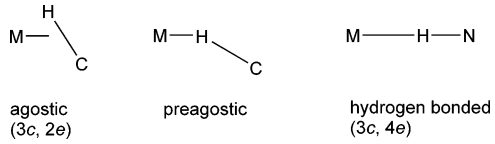

Figure 7. Modes of X−H metal coordination. Adapted from Yao, W.; Eisenstein, O.; Crabtree, R. H. *Inorg. Chim. Acta* **1997**, *254*, 105.

H_a-H_b hydrogen-bonding interaction, (c) a hydrogen bonding interaction between H_a and a rhodium-bound chloride ligand, and (d) an η^1−arene-rhodium interaction.

The "remote" or "preagostic" interaction was first fully described for C−H bonds by Albinati, Pregosin, and co-workers in 1987 (Figure 7). Although preagostic interactions involve C−H bonds and transition metals, they share many traits with hydrogen bonds. As such, the crystal structures of preagostic complexes are characterized by widened M−H−C angles (130−170°), elongated M−C distances (3.0 Å or greater), and lengthened M−H distances (2.3 Å to 2.9 Å). The ^{1}H NMR spectra of these complexes feature downfield shifts for the preagostic protons, and the associated $^{13}C-^1H$ coupling constants are typically unperturbed. The electronic similarity of preagostic (a) and hydrogen bonding (b, c) makes these effects appear very similar by ^{1}H NMR and ^{13}C NMR spectroscopy, and these hypotheses are consistent with the downfield shifts of the H_a resonances and the presence of H_a-H_b coupling in **3a**−**c**. Additionally, an η^1−arene−rhodium interaction (d) might deshield H_a, also accounting for the downfield shift of this resonance.

Literature precedent exists for all four hypotheses described above and presented in Figure 6. Although relatively few complexes feature preagostic bonding (a), the crystallographically determined C_a-Rh and H_a-Rh distances in **3a**−**c** are consistent with the reported bond lengths for such complexes.[51−60] Similarly, examples of direct hydrogen bonding (b) between metal hydrides and aryl protons are rare, but not unheard of. Gusev et al.[19] have observed direct hydrogen bonding interactions between ruthenium hydride ligands and aryl-agostic protons in structurally related pincer complexes.[61] Ample precedent exists for hydrogen bonding with halides ligated to transition metals (c),[50,62,63] and a $C_{aryl}-H\cdots Cl-Pt$ interaction was reported in a related pincer ligand complex.[64] Finally, as described in the Introduction, η^1−arene interactions (d) have been reported for a limited number of organometallic complexes.

T_1 Minimum Studies. Gusev's report of a direct $H_{aryl}-H_{metal}$ hydrogen bonding interaction involving a metal hydride ligand in a pincer ligand framework led us to consider the possibility of a H_a-H_b hydrogen-bonding interaction (b). The crystal structures of **3a**−**c** definitively ruled out such an interaction in the solid state, due to the observed *trans* arrangement of the chloride ligands (and corresponding pseudo-*trans* disposition of H_a and H_b). However, *cis*−*trans* isomerization of complexes **3a**−**c** could make this interaction possible in solution. To address this possibility, several probes were used to determine whether direct H_a-H_b hydrogen bonding was responsible for the NMR features of **3a**−**c**.

As a diagnostic test for a direct H_a-H_b interaction, the temperature-dependent T_1 values were measured for H_a and H_b in complex **3a**. The T_1 minimum for H_a was found to be 962 ms at 240 K (500 MHz). This value is not unusual for a typical aryl proton, although aryl T_1 values are notoriously variable.[65,66] The T_1 minimum for H_b was found to be 301 ms at 237 K (500 MHz), a typical value for a classical metal hydride.[46,67,68] These data argue against a direct H_a-H_b interaction, which would be expected to cause significant reduction of both T_1 values; the reported T_1 values for nonclassical metal hydride complexes are typically less than 150 ms.[46] Importantly, in the aryl-agostic pincer complex described by Gusev[19] (for which H−H bonding was determined to be significant), the observed T_1 minimum for the metal hydride was 72 ms (200 MHz).

Determination of Solution-Phase Structures. To further explore the question of whether the NMR features of **3a**−**c** were due to direct H_a-H_b bonding, several techniques were used to probe the relationship between the solid- and solution-state structures of complexes **3a**−**c**. A ^{1}H-^{1}H NOESY experiment was performed on **3b** to identify the geometry of the conformer present in solution. Crosspeaks were observed for NOE interactions between the H_b and the oxazolyl isopropyl groups, indicating that **3b** has a geometry in which both chloride ligands are *trans* to one another in solution (Figure 8). As would be expected for this geometry, no NOE was observed between H_a and H_b. These effects were also observed in a 1D NOE experiment performed on **3b**.

The solution state infrared spectrum of **3b** contains a single hydride stretching frequency ($\nu_{RhH}(CH_2Cl_2) = 2158$ cm^{-1}) and two C−N stretching vibrations ($\nu_{CN}(CH_2Cl_2) = 1655, 1643$ cm^{-1}), consistent with the C_1-symmetry of the complex.

(60) Yao, W. B.; Eisenstein, O.; Crabtree, R. H. *Inorg. Chim. Acta* **1997**, *254*, 105−111.
(61) Crabtree and others have described such hydrogen bonding interactions between metal hydrides and more traditional hydrogen bond donors, see Crabtree, R. H.; Siegbahn, P. E. M.; Eisenstein, O.; Rheingold, A. L. *Acc. Chem. Res.* **1996**, *29*, 348−354.
(62) Aullon, G.; Bellamy, D.; Brammer, L.; Bruton, E. A.; Orpen, A. G. *Chem. Commun.* **1998**, 653−654.
(63) Brammer, L.; Bruton, E. A.; Sherwood, P. *Cryst. Growth Des.* **2001**, *1*, 277−290.
(64) Albrecht, M.; Dani, P.; Lutz, M.; Spek, A. L.; van Koten, G. *J. Am. Chem. Soc.* **2000**, *122*, 11822−11833.
(65) Gèunther, H. *NMR Spectroscopy: An Introduction*; Wiley: Chichester Eng.; New York, 1980.
(66) Sanders, J. K. M.; Hunter, B. K. *Modern NMR Spectroscopy: A Guide for Chemists*, 2nd ed.; Oxford University Press: Oxford, New York, 1993.
(67) Desrosiers, P. J.; Cai, L. H.; Lin, Z. R.; Richards, R.; Halpern, J. *J. Am. Chem. Soc.* **1991**, *113*, 4173−4184.
(68) This method of determining the presence of H−H interactions has been shown to be somewhat unreliable for a family of osmium polyhydride complexes, see Desrosiers et al.[67]

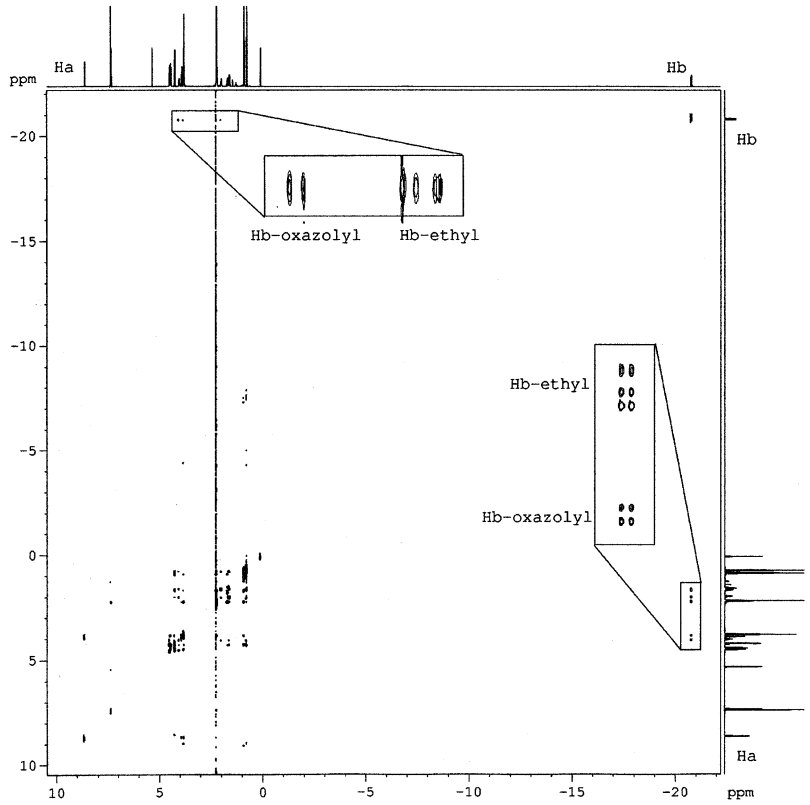

Figure 8. 2D ^{1}H-^{1}H NOESY spectrum of **3a**. Correlations between H_b and ligand protons are enlarged. No correlations between H_a and H_b were observed.

Similarly, the solid-state infrared spectrum of **3b** showed a single rhodium hydride stretching frequency (ν_{RhH}(KBr) = 2162 cm^{-1}) and two C−N stretching vibrations (ν_{CN}(KBr) = 1653, 1640 cm^{-1}). The assignment of the hydride stretching frequencies was confirmed by treatment of **1b** with D_2. This produced the deuterated analogue **3b**−**d_2**, which gave rise to shifted deuteride stretching frequencies (ν_{RhD}(CH_2Cl_2) = 1739 cm^{-1}, ν_{RhD}(KBr) = 1739 cm^{-1}, and ν_{RhD}(predicted) = 1539 cm^{-1}).[69] These data suggest that only one conformational isomer of the complex is present in solution, and that the same isomer (namely, the *trans* dichloride complex) is present in both solution and the solid states.

Variable Temperature Studies. Variable temperature NMR spectroscopy was used to assess the effect of temperature on the coupling phenomena in **3a**−**c**. A d_8-toluene solution of **3b** was cooled from 298 to 185 K in the NMR probe, and spectra were recorded every 20 K. The H_a−H_b coupling was eventually obscured by general broadening of the spectrum (presumably due to increasing solvent viscosity), but was observed in H_a, unperturbed, as low as 213 K. Furthermore, the chemical shifts of H_a and H_b did not change over the temperature regime explored in this experiment. The resonance for H_b became broad at a much higher temperature than that for H_a. It began to broaden at 275 K and the H_a−H_b coupling was completely obscured in the resonance for H_b by 233 K. No new species were frozen out at further reduced temperatures, so the broadening of H_b must be due to a fluxional process that was not slowed significantly by 185 K; we suggest that slowed rotation of the ligand-based ethyl groups is responsible for this broadening.

(69) The fact that hydride stretch does not shift upon deuteration as far as predicted by classical mechanics can be attributed to slight changes in the bond force constant between the hydride and deuteride groups.

Taken together, the crystallographic, infrared, VT NMR, and NOESY data conclusively exclude the possibility of direct H_a−H_b hydrogen-bonding interactions in **3a**−**c**. The infrared and VT NMR data confirm that these complexes exist as one major isomer in solution. The NOESY and T_1 minimum data for **3b** show that this isomer has the same geometry as that observed in the solid-state structure. As the solid-state structures of **3a**−**c** preclude any direct H_a−H_b hydrogen bonding interaction, the NMR properties of complexes **3a**−**c** do not result from direct H_a−H_b hydrogen bonding.

Probes for H_a−Cl Hydrogen Bonding. The possibility of H_a−Cl ligand bonding (c) is an attractive explanation, as this hypothesis squares with the crystal structure data and accounts for the downfield chemical shift of H_a. The crystallographic data for **3a**−**c** indicate that the H_a−Cl distances (based on calculated H_a positions) are slightly less than the sum of the van der Waals radii for H and Cl (Table 5). The H_a−Cl hydrogen bonding hypothesis was probed by chemical means, as such an interaction would be predicted to increase the acidity of H_a. Additionally, we hypothesized that addition of Lewis bases (to coordinate to H_a) or proton sources (to coordinate to Cl) might d*estroy* such a H_a−Cl ligand bond. It was found that the addition of hydrogen bond donors or acceptors had no effect on the H_a−H_b coupling. The coupling was unperturbed in CD_3OD or d_8-thf solution, and was not altered by addition of a 2-to-10-fold excess of: ionic salts (LiBr, Bu_4NBr), acetic acid, 2,6-dimethylaniline, or triethylamine. The reactivity of **3a** suggests that H_a is not sufficiently polarized to react with either acids or bases, arguing strongly against a direct electrostatic interaction between H_a and a chloride ligand.[64] Although we cannot conclusively rule out the possibility that steric shielding prevents reactions between H_a and polar reagents, this alternative seems

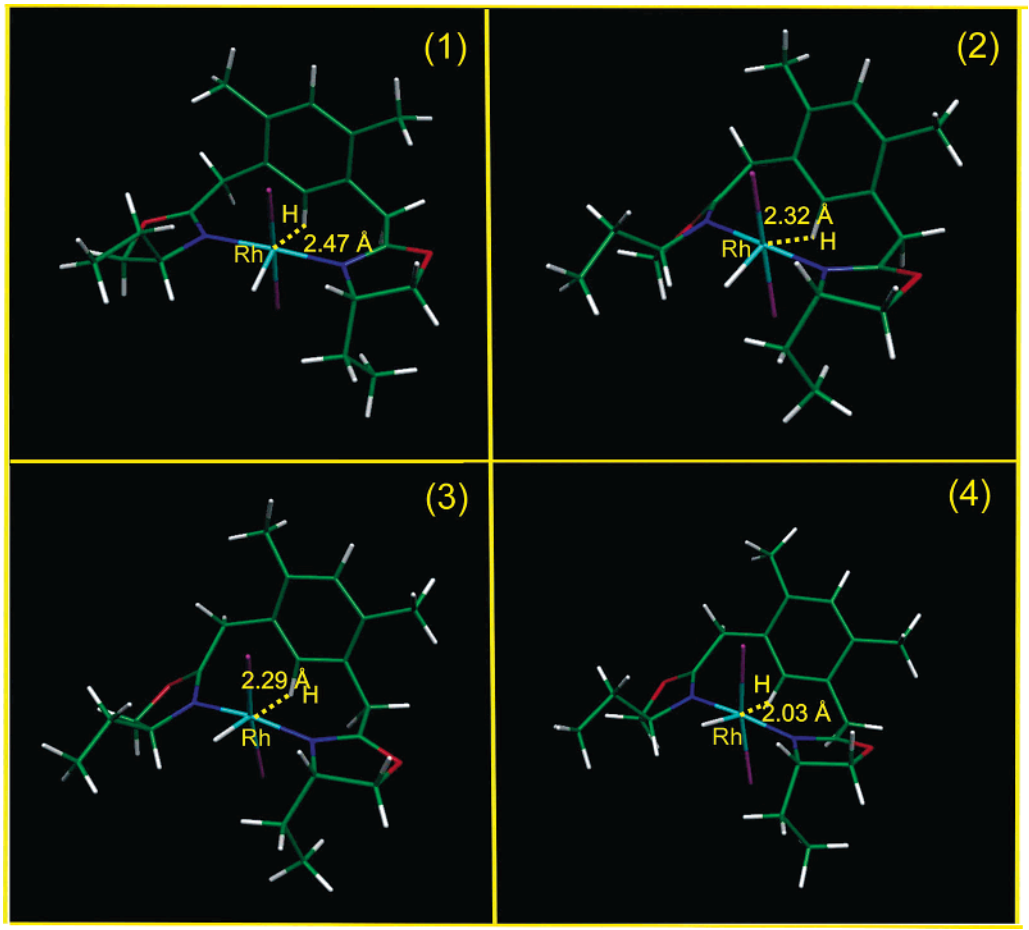

Figure 9. Snapshots of a molecular dynamics run at 500 K on complex **3a**. The four frames represent the configuration that the molecule assumes after (1) 25 fs (2) 155 fs, (3) 200 fs, and (4) 895 fs.

unlikely given the relative ease of proton transfer in the related dimeric $C_{aryl}-H\cdots Cl-Pt$ pincer complex reported by van Koten et al.[64] These reactivity data also argue against the presence of traditional agostic interactions in **3a**−**c** as alkyl and aryl agostic groups have been shown to have increased acidities.[17,70,71]

Calculations on 3a. Having ruled out not only simple agostic interactions, but also direct H_a-H_b bonding (b) and H_a-Cl bonding (c), DFT calculations were performed on complex **3a** to distinguish between possible preagostic interactions (a) in **3a**−**c** and η^1−arene interactions (d) in these complexes. Static and dynamic DFT calculations were performed with ADF2000.01[72−74] and CPMD, respectively.[75]

The calculated molecular structure for **3a** was found to be in close agreement with the structure determined by X-ray crystallography. All bond lengths and angles were calculated to be within 5% of the values determined by X-ray crystallography, with the largest deviation between the structures occurring at the $Rh-H_b$ bond (calculated length = 1.52 Å; bond length by X-ray = 1.45(7) Å). The NMR spectrum of **3a** was simulated as a second check of the calculations' accuracy. The calculated chemical shift for H_a is 8.5 ppm, quite close to the experimentally observed value of 8.9 ppm

To understand the potential fluxional properties of the system, molecular dynamics calculations were performed. The simulations were performed at temperatures of 500 and 1000 K to improve the sampling efficiency. The finite temperature behavior of the system is characterized by rather large oscillations involving H_a. In short molecular dynamics simulations of ~1 ps at 500 K, rotation of the ligand aryl ring was observed, causing the C_a-H_a vector to point toward the rhodium center (Figure 9). Due to this rotation, the $Rh\cdots H_a$ distance was found to oscillate between 2.97 and 2.03 Å. This motion could be interpreted as optimizing the geometry for a preagostic interaction by widening the C_a-H_a-Rh angle (for **3a**, this angle is 74.3°, while preagostic interactions generally feature angles of 130−170°).

Interestingly, as the calculated $Rh-H_a$ distance shortens, the calculated chemical shift for the H_a resonance moves downfield (Table 6). However, correlations between H_a and H_b were observed neither during this calculation nor in a 0.7 ps calculation at 1000 K. Notably, elongation of the aryl H_a-C_a bond, as would be predicted for a traditional agostic interaction, was not observed during these simulations. Additionally, no evidence of a $H_a\cdots Cl$ interaction (c) was observed.

To better understand the H_a-H_b coupling and the lack of $Rh-H_a$ coupling, these coupling constants were calculated for the optimized geometry and for each of the four frames of the

(70) Speckman, D. M.; Knobler, C. B.; Hawthorne, M. F. *Organometallics* **1985**, *4*, 1692−1694.
(71) Kanamori, K.; Broderick, W. E.; Jordan, R. F.; Willett, R.; Legg, J. I. *J. Am. Chem. Soc.* **1986**, *108*, 7122−7124.
(72) Baerends, E. J.; Ellis, D. E.; Ros, P. *Chem. Phys.* **1973**, *2*, 41−51.
(73) Baerends, E. J.; Ros, P. *Chem. Phys.* **1973**, *2*, 52−59.
(74) te Velde, G.; Baerends, E. J. *J. Comput. Phys.* **1992**, *99*, 84−98.
(75) Hutter, J.; Ballone, P.; Bernasconi, M.; Focher, P.; Fois, E.; Goedecker, S.; Parrinello, M.; Tuckerman, M. *CPMD*; Max-Planck-Institut fuer Festkörperforschung, Stuttgart and IBM Research Laboratory, Zürich, 1998.

Table 6. Selected Interatomic Distances (Å), Calculated Chemical Shifts (ppm), and Calculated Coupling Constants (Hz) for Selected Frames of the Molecular Dynamics Simulation on **3a** at 500 K

	optimized structure	frame 1	frame 2	frame 3	frame 4
H_a Shift	8.5 ppm	8.4 ppm	7.7 ppm	11.2 ppm	11.1 ppm
J (H_a-H_b)	1.8	1.7	6.6	10.4	12.0
J (Rh$-H_a$)	1.0	1.0	0.5	0.4	1
C_a-H_a Distance	1.09 Å	1.05 Å	1.15 Å	1.04 Å	1.09 Å
Rh$-H_a$ Distance	2.72 Å	2.47 Å	2.32 Å	2.29 Å	2.03 Å

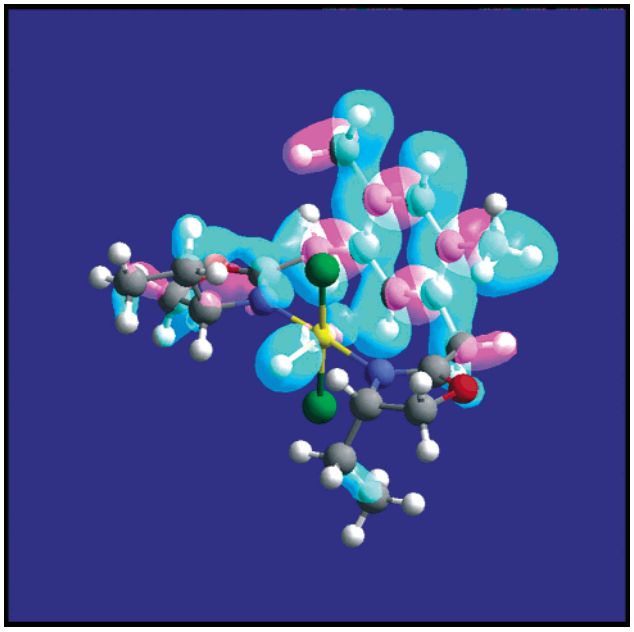

Figure 10. Contour plot of HOMO-20 orbital of the optimized gas-phase geometry of complex **3a**. The contours are given at ±0.02 au.

molecular dynamics simulation (Table 6). In excellent agreement with the experimental results, an extremely small Rh$-H_a$ coupling constant is predicted by the calculations. This coupling constant changes somewhat between different frames of the dynamics, but its value never increases above 1 Hz. Not surprisingly, the H_a-H_b coupling is dramatically affected by the distance between these two protons in the dynamics calculations. In the optimized gas-phase geometry, the calculated H_a-H_b coupling constant of 1.8 Hz is in good agreement with the experimental results. This coupling constant increases as the H_a-H_b distance decreases during the molecular dynamics run, reaching a value of 12 Hz after 895 fs of dynamics.

The excellent agreement between the calculated and experimental ^{1}H NMR chemical shifts and the coupling constants associated with H_a (δ(expt) = 8.9 ppm, δ(calc) = 8.5 ppm; J_{H-H}(expt) = 2.5 Hz, J_{H-H}(calc) = 1.8 Hz; J_{Rh-H}(expt) = <1 Hz, J_{Rh-H}(calc) = <1 Hz) supports the accuracy of these calculations. Therefore, to understand the origin of the H_a-H_b coupling in **3a**–**c** we performed a visual inspection of the Kohn–Sham orbitals. Despite the calculated geometrical changes at high temperature, no molecular orbitals consistent with a preagostic interaction between H_a and Rh were found in any of the dynamics calculations. Inspection of the one-electron Kohn–Sham orbitals of the optimized gas-phase geometry of **3a** revealed that the diffuse HOMO-20 orbital connects H_a with H_b via the complex's σ-bonding network (Figure 10). However, in a preagostic bond H_a should act as a weak acid toward Rh, as in a classical hydrogen-bonding arrangement (vide infra). The diffusivity of the calculated HOMO-20 orbital and its lack of electron density on Rh are not consistent with a preagostic bond, and we believe that the NMR coupling of H_a and H_b must occur via orbitals other than the HOMO-20.

In contrast, the electronic structure of **3a** supports the hypothesis that weak η^1–arene interactions exist in complexes **3a**–**c**. The calculated HOMO−8 and HOMO−9 orbitals of **3a** show direct overlap of the C_a-based p-orbital with rhodium's orbitals (Rh-p_z in HOMO−9, Rh-d_{xz} in HOMO−8, Figure 11). Importantly, none of these orbitals has any density at H_a. This suggests that C_a alone, rather than the C_a-H_a bond, interacts directly with the rhodium center. This finding is consistent with the conclusion that **3a**–**c** feature weak η^1–arene interactions, rather than any of the alternative bonding modes (a–c) that involve direct interaction of H_a with rhodium or its ligands.

Discussion

Experimental results were used to rule out traditional agostic interactions, direct through-space H_a-H_b hydrogen-bonding interactions (b), and hydrogen bonding between H_a and a rhodium-bound chloride ligand (c) as the source of the unique NMR features of **3a**–**c**. DFT calculations suggested that weak η^1–arene interactions (d) are more likely to be present in **3a**–**c** than preagostic bonding (a). A survey of the exisiting preagostic and η^1–arene bonding literature supports this conclusion.

Preagostic bonding has been reported for complexes with long M–H and M–C distances.[51,53–57,76] Like those in **3a**–**c**, the interacting protons of these preagostic complexes are characterized by low field proton NMR shifts and generally unperturbed C–H coupling constants.[53,58,77] The downfield shifts of the H_a protons ($\Delta\delta$ 1.8 ppm) in **3a**–**c** clearly fit into this category of strongly perturbed resonances. Also, as with **3a**–**c**, in the literature examples of preagostic complexes with NMR active metals or ligands, the magnitude of the coupling between these nuclei and the preagostic protons is usually less than that observed in "true" agostic complexes. The M–H distances of the structurally characterized preagostic complexes range from 2.3 to 2.9 Å, similar to those observed in **3a**–**c**.[60]

Despite the similarities between the reported cases of preagostic bonding and the data for **3a**–**c**, several important differences remain. All the definitive examples of preagostic bonding exist in d^8 metal complexes with square planar ligand arrangements.[51,53–57,76] As the *filled* d_{z^2} orbitals of these d^8 complexes are available for hydrogen bonding in the axial ligand site, preagostic bonds have been formulated as primarily electrostatic interactions.[78] This conclusion is supported by the near linearity of preagostic bonds (C–H–M bond angles are generally 130–170°).[60] In contrast to the previously reported examples of preagostic bonding, the d_{z^2} orbitals of **3a**–**c** (d^6) are *empty*. Correspondingly, the C–H–M bond angles in complexes **3a**–**c** (74–76°) are much more acute than would

(76) Schwartz, D. J.; Ball, G. E.; Andersen, R. A. *J. Am. Chem. Soc.* **1995**, *117*, 6027–6040.
(77) Low field shifts of known preagostic protons may result, in part, from anisotropic effects from the metal d-orbitals, but the magnitudes of the relevant shifts (1–3.5 ppm) are too great to be explained by anisotropic effects alone.
(78) It should be noted that d^8 square-planar complexes are also 16-electron species, and hence, theoretically also available to accept electron density in a 3*c*-2*e* fashion. However, as noted by Crabtree and Eisenstein,[60] the only vacant metal-based orbital of appropriate symmetry is the p_z, which is high in energy and probably not a major contributor to the overall bonding interaction.

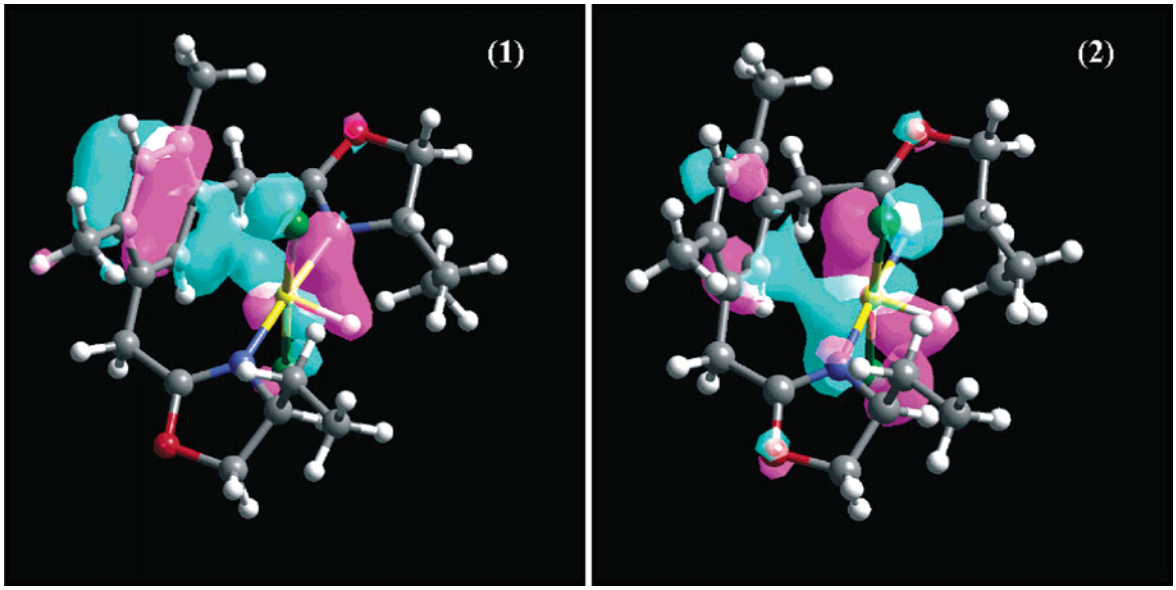

Figure 11. Contour plots of: (1) HOMO-8 and (2) HOMO-9 orbitals of the optimized gas-phase geometry of complex **3a**. The contours are given at ±0.02 au.

be expected for 3*c*−4*e* interactions. Given this important difference and the results of our calculations, we conclude that the bonding in complexes **3a**−**c** must involve η^1−arene coordination.

The geometric and spectroscopic features of **3a**−**c** are in excellent agreement with the few reported examples of weak π-type η^1−arene coordination to transition metals.[16,24−26,28,29] Like ruthenium-based η^1−arene complexes recently reported by Pregosin et al.,[25] the aryl carbons of **3a**−**c** are found to resonate somewhat upfield of the expected shift for typical aryl carbons. The $Rh^{III}-C_a$ distances in **3a**−**c** (2.61−2.63 Å) are quite similar to the Ru^{II}−C(*ipso*) distances (2.62−2.63 Å) in the Pregosin complexes, and somewhat shorter than the Pd^0−C(*ipso*) distance (2.68 Å) reported recently by Fink et al.[24] Using the Pauling equation for bond order with a radius of 1.34 Å for rhodium, the Rh−C_a bond orders in **3a**−**c** range from 0.14 to 0.15, values consistent with the weak nature of the π η^1−arene interaction.[79,80] Also consistent with the limited previous reports of π-type η^1−arene coordination, the aryl C−C bond distances and angles in **3a**−**c** show essentially no evidence of ring expansion or bond localization; this is consistent with the extremely weakly bonding nature of these interactions.[81]

Interesting contrasts can be drawn between the weak η^1−arene interactions in rhodium complexes **3a**−**c** and the bonding interactions observed in related, previously reported pincer complexes. Several groups have reported platinum,[27] ruthenium,[19−23] and rhodium[17,18] complexes of PCP and NCN pincer ligands that contain weak bonding interactions between aryl backbone groups and the metal centers. While these complexes are structurally similar to ours, none feature the π-type η^1−arene interactions that we observe. Instead, most of these complexes involve η^2−C−H aryl agostic bonding.[17−23,82] Interestingly, van Koten et al.[27] have described platinum NCN pincer complexes containing strong η^1−arene bonding interactions with the ligand backbone. However, unlike complexes **3a**−**c**, the η^1−arene bonds in the van Koten complexes are strongly polarized and of the σ-type. These complexes are best described as Wheland-type arenium complexes and have structural and spectroscopic features quite different from those of the π-type η^1−arene complexes **3a**−**c**.

The difference between interaction modes in the previously reported pincer complexes and ours can be attributed to the fact that complexes **3a**−**c** feature 10-membered bidentate chelate rings while the others are eight-membered.[17,19−23,27] The larger chelate rings in our complexes enforce a greater distance between the rhodium centers and the arene C−H bonds, making the relatively close contacts (and correspondingly stronger bonding interactions) necessary for η^2−C−H aryl agostic bonding or σ-type η^1−arene complexation more difficult to achieve. Additionally, as compared to the metal centers in the known η^2−C−H aryl agostic complexes (Ru(II) and Rh(I)), our more highly oxidized metal centers have a lesser potential for back-bonding. We have found that weak π-type η^1−arene interactions can be observed in complexes with rigid ligand frameworks that preclude coordination of rhodium's empty coordination site by strong ligands. Our observations suggest that a range of η^1−arene interactions are possible, depending on structural constraints imposed by the ligands.

Experimental Section

General Procedures. Unless otherwise noted, reactions and manipulations were performed at 23 °C in an inert atmosphere (N_2) glovebox, or using standard Schlenk and high-vacuum line techniques. Glassware was dried overnight at 150 °C before use. High-pressure reactions were performed in steel reaction vessels purchased from the Parr Instrument Company. All NMR spectra were obtained using Bruker AMX-400, AM-400, or DRX-500 MHz spectrometers. Except where noted, all NMR spectra were acquired at room temperature. Infrared

(79) Shriver, D. F.; Atkins, P. W.; Langford, C. H. *Inorganic Chemistry*, 2nd ed.; W. H. Freeman: New York, 1994.
(80) Pauling, L. *The Nature of the Chemical Bond and the Structure of Molecules and Crystals; an Introduction to Modern Structural Chemistry*, 3rd ed.; Cornell University Press: Ithaca, N. Y., 1960.
(81) The high degree of thermal disorder in the structure for **3b** may explain the slight perturbations in the C−C bond distances for this complex.
(82) The Ru complexes reported by Gusev et al.[19] contain both aryl agostic interactions and direct H−H bonding. As described in the results section, direct H_a-H_b bonding is not possible in **3a**−**c** because of the *trans* geometries of these complexes.

(IR) spectra were recorded using samples prepared as KBr pellets or as CH_2Cl_2 solutions and spectral data are reported in wavenumbers. Elemental analyses were performed at the University of California, Berkeley Microanalytical facility on a Perkin-Elmer 2400 Series II CHNO/S Analyzer.

Materials. Unless otherwise noted, reagents were purchased from commercial suppliers and used without further purification. Pentane, toluene, methylene chloride, and benzene (Fisher) were passed through columns of activated alumina (type A2, size 12 × 32, Purifry Co.) under nitrogen pressure and sparged with N_2 prior to use. Deuterated solvents (Cambridge Isotope Laboratories) were purified by vacuum transfer from the appropriate drying agent (Na/Ph_2CO for C_6D_6, CaH_2 for CD_2Cl_2, NaOEt-d_5 for d_6-ethanol). Rhodium complexes **2a**−**c** were prepared as described previously.[37]

General Procedure for Synthesis of Rhodium Complexes 3a−c. A high-pressure steel reaction vessel was charged with the orange-red rhodium complex **2** (0.11−0.24 mmol) in 20−30 mL benzene. The vessel was pressurized with 35 atm H_2 and heated to 75 °C for 10 h. After this time, the resulting yellow solution was filtered, quickly pumped down, and finally washed with pentane (3 × 7 mL) to yield a spectroscopically and analytically pure yellow powder.

[$RhCl_2$(H){(*S,S*)-et-Benbox(Me_2)H}] (3a). Yield = 57 mg, 85%. Anal. Calcd for $C_{20}H_{29}Cl_2N_2O_2Rh$: C, 47.73; H, 5.81; N, 5.56. Found: C, 47.64; H, 5.49; N, 5.30. IR (KBr): 2169 (ν_{RhH}), 1656, 1642 (ν_{CN}). ^{1}H NMR (300 MHz, C_6D_6): δ 8.88 (d, 1H, C*H*, J_{H-H} = 2.5 Hz), 7.18 (s, 1H, C*H*), 3.99 (m, 1H, ox−C*H*), 3.83−3.39 (m, 9H), 2.08 (s, 3H, CH_3), 1.98 (s, 3H, CH_3), 1.80 (m, 4H, Et−CH_2), 0.64 (t, 3H, Et−CH_3), 0.51 (t, 3H, Et−CH_3), −20.76 (dd, 1H, Rh−*H*, J_{H-H} = 2.5 Hz, $^1J_{Rh-H}$ = 22.1 Hz). ^{13}C{^{1}H} NMR (125 MHz, C_6D_6): 172.1, 171.3, 139.3, 137.9, 129.5, 128.6, 128.2, 118.5, 72.1, 71.9, 68.0, 64.9, 33.7, 33.5, 26.6, 26.4, 8.2, 8.1.

[$RhCl_2$(H){(*S,S*)-ip-Benbox(Me_2)H}] (3b). Yield = 47 mg, 45%. Anal. Calcd for $C_{22}H_{33}Cl_2N_2O_2Rh$: C, 49.73; H, 6.26; N, 5.27. Found: C, 49.38; H, 5.97; N, 4.88. IR (KBr, cm^{-1}): 2162 (ν_{RhH}), 1651, 1642 (ν_{CN}). IR(CH_2Cl_2) = 2158 cm^{-1} (ν_{RhH}), 1643, 1655(ν_{CN}). ^{1}H NMR (300 MHz, C_6D_6): δ 8.90 (d, 1H, C*H*, J_{H-H} = 3.1 Hz), 7.19 (s, 1H, C*H*), 4.06 (m, 1H, ox−C*H*), 3.92 (m, 1H, ox−C*H*), 3.80 (d, 1H, CH_2, $^2J_{H-H}$ = 15.2 Hz), 3.74−3.40 (m, 7H), 2.93 (sept, 1H, ^{i}Pr−C*H*), 2.93 (sept, 1H, *i*-Pr−C*H*), 2.06 (s, 3H, CH_3), 1.98 (s, 3H, CH_3), 0.95 (t, 3H, ^{i}Pr−CH_3), 0.62 (t, 3H, *i*-Pr−CH_3), 0.42 (t, 3H, *i*-Pr−CH_3), 0.41 (t, 3H, *i*-Pr−CH_3), −20.81 (dd, 1H, Rh−*H*, J_{H-H} = 3.1 Hz, $^1J_{Rh-H}$ = 22.1 Hz). ^{13}C{^{1}H} NMR (126 MHz, C_6D_6): δ 172.3, 136.28, 136.26, 136.21, 121.46, 74.15, 71.78, 68.51, 68.20, 30.93, 30.18, 28.71, 28.09, 18.39, 14.20.

[$RhCl_2$(H){dm-Benbox(Me_2)H}] (3c). Yield = 94 mg, 75%. Anal. Calcd for $C_{20}H_{29}Cl_2N_2O_2Rh$: C, 47.73; H, 5.81; N, 5.57. Found: C, 47.61; H, 5.85; N, 5.51. IR (KBr): 2197 (ν_{RhH}), 1642 (ν_{CN}). ^{1}H NMR (300 MHz, C_6D_6): δ 9.03 (d, 1H, C*H*, $^2J_{H-H}$ = 3.3 Hz), 7.18 (s, 1H, C*H*), 3.69 (d, 2H, CH_2, $^2J_{H-H}$ = 16.6 Hz), 3.46 (m, 6H, ox-CH_2, CH_2), 2.01 (s, 6H, CH_3), 1.49 (s, 6H, ox-CH_3), 1.28 (s, 6H, ox-CH_3), −19.70 (dd, 1H, Rh-*H*, J_{H-H} = 3.3 Hz, $^1J_{Rh-H}$ = 18.8 Hz). ^{13}C{^{1}H} NMR (126 MHz, $CDCl_3$): δ 170.7, 136.6, 134.1, 130.5, 121.6, 79.1, 70.0, 31.4, 29.1, 29.0, 18.7.

NMR Reactivity Studies of 3a. The rhodium complex **3a** (4.0 mg, 0.079 mmol) and 1,4-dimethoxybenzene (standard, 2.7 mg, 0.019 mmol) were dissolved in 300 μL of the appropriate deuterated solvent (CD_3OD, d_8-thf, or CD_2Cl_2). A 2-to-10-fold excess of the second reagent (acetic acid, amine base, etc.) was added, and the resulting solution was transferred to a medium-walled NMR tube. The solution was degassed, and the tube was flame-sealed under vacuum. The sample was warmed to room temperature and an initial ^{1}H NMR spectrum was recorded. The tube was heated at 75 °C in an oil bath, cooled to room temperature and a ^{1}H NMR spectrum was recorded. The progress of the reaction was analyzed by integrating the product signals against the internal standard. Reactions were not heated above 75 °C, as decomposition of the starting material was observed at higher temperatures. Attempts to avoid formation of decomposition products by running the reactions under an atmosphere of H_2 gas were unsuccessful.

X-ray Structure Determinations. *General Considerations.* X-ray crystal structures were obtained by Fred Hollander and Allan Oliver at the UCB X-ray facility (CHEXRAY). Crystals were mounted on glass fibers using Paratone N hydrocarbon oil. All measurements were made on a SMART[83] CCD area detector with graphite monochromated Mo−Kα radiation (λ = 0.71069 Å). The data were collected with a detector position of 60.00 mm. Data were integrated by the program SAINT,[84] and were corrected for Lorentz and polarization effects. Data were analyzed for agreement and possible absorption using XPREP.[85] The structures were solved by direct methods[85] and expanded using Fourier techniques.[86]

[$RhCl_2$(H){(*S,S*)-et-benbox(Me_2)H}] (3a). X-ray quality crystals of **3a** were collected by cooling a toluene solution of **3a** to −30 °C. The data were collected using 10-s frames with an ω scan of 0.3°. Empirical absorption corrections based on comparison of redundant and equivalent reflections were applied using XPREP (*Tmax* = 0.86, *Tmin* = 0.77). The maximum peak in the final difference map was 0.36 e$^-$/Å^3, and the minimum peak was −0.24 e$^-$/Å^3. The correct enantiomorphs of the molecule and space group were determined by comparison of Friedel pairs.

[$RhCl_2$(H){(*S,S*)-ip-benbox(Me_2)H}] (3b). X-ray quality crystals of **3b** were collected by cooling a toluene/pentane solution of **3b** to −30 °C. The data were collected using 10-s frames with an ω scan of 0.3°. Empirical absorption corrections based on comparison of redundant and equivalent reflections were applied using SADABS[87] (*Tmax* = 0.93, *Tmin* = 0.82). The maximum peak in the final difference map was 0.38 e$^-$/Å^3, and the minimum peak was −0.28 e$^-$/Å^3. The correct enantiomorphs of the molecule and space group were determined by comparison of Friedel pairs.

[$RhCl_2$(H){dm-benbox(Me_2)H}] (3c). X-ray quality crystals of **3c** were collected by cooling a toluene/pentane solution of **3c** to −30 °C. The data were collected using 10-s frames with an ω scan of 0.3°. Empirical absorption corrections based on comparison of redundant and equivalent reflections were applied using SADABS[87] (*Tmax* = 0.97, *Tmin* = 0.62). The maximum peak in the final difference map was 0.81 e$^-$/Å^3, and the minimum peak was −0.97 e$^-$/Å^3.

Computational Details. The static DFT calculations were performed with the program ADF2000.01,[72−74] whereas DFT-based molecular dynamics simulations were performed with the code CPMD.[75] The structure of complex **3a** was optimized for three different spin states using the Amsterdam Density Functional (ADF) program.[72−74] The electronic configurations of the molecular systems were described by a triple-STO basis set on the transition metal center for the ns, np, nd, (n+1)s, and (n+1)p valence shells, whereas a double-STO basis set was used for Cl (2s, 2p), C (2s 2p), N (2s, 2p), O(2s, 2p), and H(1s). The inner shells of the atoms were treated with the frozen core approximation. Energy differences were calculated including Becke's exchange[88] and Perdew's correlations gradient corrections.[89] First-order scalar relativistic corrections[90,91] were added to the total energy for the rhodium atom.

(83) *Area-Detector Software Package*; Siemens Industrial Automation, Inc.: Madison, WI, 1995.
(84) *SAX Area-Detector Integration Program*, V4.024; Siemens Industrial Automation Inc.: Madison, WI, 1995.
(85) *XPREP*, v. 5.03, Part of the SHELXTL Crystal Structure Determination; Siemens Industrial Automation Inc.: Madison, WI, 1995.
(86) Beurskens, P. T.; Admiraal, G.; Beurskens, G.; Bosman, W. P.; de Gelder, R.; Israel, R.; Smits, J. M. M. 1994. *The DIRDIF-94 program system*, Technical Report of the Crystallography Laboratory; University of Nijmegen: The Netherlands.
(87) *Siemens Area Detector Absorption correction program*, V. 205; George Sheldrick, 2002.
(88) Becke, A. *Phys. Rev. A* **1988**, *38*, 3098−3100.
(89) Perdew, J. P.; Zunger, A. *Phys. Rev. B* **1981**, *23*, 5048−5079.
(90) Snijeders, J. G.; Baerends, E. J. *J. Mol. Phys.* **1978**, *36*, 1789−1804.
(91) Snijeders, J. G.; Baerends, E. J.; Ros, P. *J. Mol. Phys.* **1979**, *38*, 1909−1929.

Calculations of the NMR chemical shifts of the most relevant atoms were also performed with ADF2000.01[92−94] performing single-point calculations on the gas-phase optimized geometry and on some frames of the molecular-dynamics simulations generated with CPMD.[75] Chemical shifts were calculated with a triple STO basis set on Rh, while for all the other elements these were calculated with a double STO basis set considering all the core and the valence electrons. In both cases ZORA[95−97] relativistic corrections were added.

The singlet structure of **3a** was also optimized, using the program CPMD. In the CPMD calculations, an analytical local pseudopotential was used for hydrogen, and nonlocal, normconserving pseudopotentials of the Martins-Troullier type[98] were employed for all the other elements. Angular momentum components up to l_{max} = S have been included for carbon, nitrogen and oxygen and l_{max} = P for chlorine atoms. For rhodium, a semicore pseudopotential (l_{max} = D) for which the $4s^2 4p^6 4d^7$ and $5s^2$ valence electrons are treated explicitly was constructed. All pseudopotentials, with the exception of that of rhodium, were transformed to a fully nonlocal form using the scheme developed by Kleinman and Bylander.[99] For rhodium, the nonlocal part of the pseudopotential was integrated numerically using a Gauss-Hermite quadrature. The same exchange-correlation functional was used as in the ADF calculations.

All calculations were performed in a periodically repeated simple cubic cell of 16 Å. A kinetic energy cutoff of 70 Ry was used for the expansion of the one-electron wave functions. The classical equations of motion were integrated with a velocity Verlet algorithm with a time step of 0.1 fs and a fictitious mass for the electronic degrees of freedom of μ = 400 au.

Acknowledgment. We are grateful to Professors Paul Pregosin (ETH Hönggerberg), Odile Eisenstein (Université de Paris-Sud), and Richard Andersen (UC Berkeley) for stimulating discussions about the nature of the interactions in **3a**−**c**. Drs. Fred Hollander and Allen Oliver at the UCB X-ray diffraction facility (CHEXRAY) are acknowledged for determination of the crystal structures of **3a**−**c**. Part of this work was carried out under the auspices of a CRADA project, administered by the Lawrence Berkeley National Laboratory under contract no. DE-AC03-76SF00098, in cooperation with the E. I. DuPont Co, and funded under the Initiatives for Proliferation Prevention Program of the U.S. Department of Energy; it was also supported in its later stages by NSF grant CHE-0345488 (to R. G. B.). M. G. thanks the Deutsche Forschungsgemeinschaft for a Postdoctoral Fellowship. J. R. K. thanks the National Science Foundation for a Predoctoral Fellowship.

Supporting Information Available: Parameters for 2D NMR experiments performed on **3a**−**c** and X-ray structure data (PDF). This material is available free of charge via the Internet at http://pubs.acs.org.

JA047665B

(92) Schreckenbach, G.; Ziegler, T. *J. Phys. Chem.* **1995**, *99*, 606−611.
(93) Schreckenbach, G.; Ziegler, T. *Int. J. Quantum. Chem.* **1997**, *61*, 899−918.
(94) Wolff, S. K.; Ziegler, T. *J. Chem. Phys.* **1998**, *109*, 895−905.
(95) Ziegler, T.; Snijders, J. G.; Baerends, E. J. *J. Chem. Phys.* **1981**, *74*, 1271−1284.
(96) van Lenthe, E.; Baerends, E. J.; Snijders, J. G. *J. Chem. Phys.* **1994**, *101*, 9783−9792.
(97) van Lenthe, E.; Baerends, E. J.; Snijders, J. G. *J. Chem. Phys.* **1996**, *105*, 6505−6516.
(98) Trouiller, M.; Martins, J. L. *Phys. Rev. B* **1991**, *43*, 1993−2006.
(99) Kleinmann, L.; Bylander, D. M. *Phys. Rev. Lett.* **1982**, *48*, 1425−1428.